THEORETICAL ANALYSIS OF THE ICE CRYSTAL SIZE DISTRIBUTION IN FROZEN AQUEOUS SPECIMENS

GUNNAR KOPSTAD AND ARNLJOT ELGSAETER
Division of Biophysics, University of Trondheim, Trondheim, Norway

ABSTRACT To estimate theoretically how suited different freezing techniques are for freezing of freeze-etch specimens, it is necessary to know the relationship between specimen cooling rate and the resulting average ice crystal size. Using a somewhat simplified theoretical analysis, we have derived the approximate ice crystal size distribution of nonvitrified frozen aqueous specimens frozen at different cooling rates. The derived size distribution was used to calculate the relationship between relative change in average ice crystal size, $(\overline{\Delta l/l})$, and relative change in specimen cooling rate $\Delta(dT/dt)/(dT/dt)$. We found this relationship to be $(\overline{\Delta l/l}) = -k \cdot \Delta(dT/dt)/(dT/dt)$ where $k = 1.0$ when specimen solidification takes place at about -6°C, and $k \simeq 1.3$ when it takes place at about -40°C.

INTRODUCTION

Ice crystal growth during specimen freezing represents one of the main limitations of freeze-etch electron microscopy. The specimen freezing technique that yields the smallest ice crystals normally gives rise to the most useful electron micrographs. The importance of using a high cooling rate during specimen freezing to obtain small ice crystals has long been recognized (Moor, 1964). However, to evaluate the practical importance of a certain increase in specimen cooling rate, the mathematical relationship between ice crystal size distribution and specimen cooling rate must be known. Using a somewhat simplified theoretical analysis we have derived the approximate ice crystal size distribution of aqueous specimens frozen at different cooling rates. To our knowledge no other theoretical study addressing itself to this problem has been published.

GLOSSARY

A_{exp} experimentally determined fracture plane area of an ice crystal.
$a_1(T_0), a_2(T_0)$ coefficients in Taylor expansion of log $J(T)$ around temperature T_0.
$b_1(T_0), b_2(T_0)$ coefficients in Taylor expansion of log $U(T)$ around temperature T_0.
C_1, C_2 mathematical expressions given by Eq. 5 and 6, respectively.
I_i ($i = 1, 2, 3$ and 4) mathematical expressions given by Eqs. 12, 17, 24, and 29, respectively.
$I_5(T_S) \equiv (\overline{l/\lambda})_V$.
$J(T)$ ice crystal nucleation rate.
$k(T_S)$ proportionality factor relating relative change in specimen cooling rate and relative change in ice crystal diameter.
l ice crystal diameter.
$(\overline{l/\lambda})_N$ number average ice crystal diameter (dimensionless).
$(\overline{l/\lambda})_V$ volume average ice crystal diameter (dimensionless).
$N(T_S)$ total number of ice crystals per unit volume in the solidified specimen.
$P_N(i)$ ($i = T, l, l/\lambda$) the number of ice crystals formed per unit volume in the interval $(i, i + di)$.
$P_N^A(l)$ average number of fractured ice crystals with diameter in the interval $l, l + dl$ per unit fracture plane area.
$P_N^A(r)$ relative number of ice crystal fracture plane with radius r in the interval $r, r + dr$.
$P_A^A(r/\lambda)$ area fraction of the specimen freeze-fracture plane made up of ice crystals with fracture plane radius in the interval $r/\lambda, r/\lambda, + (dr)/\lambda$.
$P_A^A(r/\eta)_{exp}$ experimentally determined area fraction $P_A^A(r/\lambda)$.
$P_V(l/\lambda)$ solidified specimen volume fraction made up of ice crystals with diameter in the interval $l/\lambda, l/\lambda + dl/\lambda$.
$P(l; r)_i$ ($i = I, II$) probability of getting an ice crystal fracture plane with radius r provided that the fracture goes through an ice crystal with diameter l.
r radius of an ice crystal fracture plane.
T temperature.
T_M specimen melting temperature.
T_N nucleating temperature of an ice crystal.
T_S specimen solidification temperature.
$\Delta T \equiv T_N - T$.
t time.
$U(T)$ ice crystal growth rate.
x integration variables or mathematical expressions defined in Eqs. 36 and 51.
$\alpha(T_S, T) \equiv 1 - \beta$.
$\alpha_n(T_S, T)$ ($n = 0, 1, 2 \ldots$) nth approximation of α.
$\beta(T_S, T)$ solidified volume fraction of the specimen.
δ Dirac's delta-function.
η parameter chosen experimentally according to Eq. 53.
λ characteristic length of the physical problem being analyzed (Eq. 32).
ξ parameter depending on the relationship between the ice crystal growth direction and the orientation of the ice crystal lattice axes.

THEORY

When the temperature of an aqueous specimen is reduced below the specimen's melting point, ice crystals may begin to grow from a few special nucleation sites (heterogeneous nucleation) or the water molecules

Dr. Kopstad's current address is the Department of Pathology, Regional Hospital, N-7000 Trondheim, Norway.

themselves may give rise to the nucleation sites (homogeneous nucleation). These processes may occur simultaneously, but in most biological specimens the nucleation process appears to be mainly homogeneous (Mazur, 1966).

During homogeneous nucleation the nuclei form spontaneously as a result of thermal movement of the water molecules. For the probability of further growth of a given nucleus to exceed the probability of size reduction, the nucleus must exceed a certain critical size (Gibbs, 1928), which is temperature dependent and decreases as the temperature is lowered. At about −40°C the critical size equals the average water molecule cluster size. Liquid water below about −40°C can be viewed as consisting fully of ice crystal nuclei with size exceeding the critical size. Below about −40°C solidification of liquid water therefore takes place without any significant ice crystal growth. This is commonly referred to as specimen vitrification. Vitrification of pure liquid water and aqueous specimens has been reported (Venkatesh et al., 1974; Brüggeller and Mayer, 1980). True vitrification, however, occurs to at most a minor fraction of specimens frozen using freezing methods well suited for freeze-etch electron microscopy.

In the unsolidified parts of the specimen there is, at any temperature below the specimen melting temperature, a certain probability of formation of ice crystal nuclei with size above the critical value. This implies that the time between ice crystal nucleation and full specimen solidification, i.e., the time interval in which an ice crystal can grow, will vary from ice crystal to ice crystal. The longer this time interval is, the larger the associated ice crystal in the fully solidified specimen will be. The ice crystals of a frozen aqueous specimen therefore exhibit a size distribution.

Specimen Solidification

We will assume in the following that the nucleation process is homogeneous, that vitrification can be ignored, and that the specimen cooling rate, $|dT/dt|$, is kept constant throughout the specimen during the freezing process. We will further assume that the average number of ice crystal nuclei per unit time and unit volume in the liquid part of the specimen (the nucleation rate), $J(T)$, can, through Taylor expansion of $\log J(T)$ around temperature T_0, be expressed as

$$J(T) = J(T_0) \cdot 10^{-a_1(T_0)\cdot(T-T_0)-a_2(T_0)\cdot(T-T_0)^2} \quad (1)$$

for $T < T_M$ where T_M is the specimen melting temperature and $T - T_0 \lesssim 5$°C. Likewise we will assume that the ice crystal growth rate, $U(T)$, can be expressed as

$$U(T) = U(T_0)\, 10^{+b_1(T_0)\cdot(T-T_0)-b_2(T_0)\cdot(T-T_0)^2} \quad (2)$$

where $T < T_M$ and $T - T_0 \lesssim 5$°C. Numerical values of $a_1(T_0)$, $a_2(T_0)$, $b_1(T_0)$, and $b_2(T_0)$ for pure water obtained from the data summarized by Riehle (1968) are shown in Table I. Parameters a_1, a_2, b_1, and b_2 have been determined by requiring that the deviation between the graphs presented by Riehle (1968) and the expressions given in Eqs. 1 and 2 is zero for both $T = T_0$ and $T - T_0 = 5$°C. Note that parameters $J(T_0)$, $a_1(T_0)$, $a_2(T_0)$, $U(T_0)$, $b_1(T_0)$, and $b_2(T_0)$ generally are solute dependent.

Assuming that the ice crystal growth rate is the same in all directions relative to the ice crystal lattice axes, the ice crystal diameter, $l(T)$, of an ice crystal that nucleated at temperature T_N will, at temperature T, be

$$l(T) = 2\int_T^{T_N} U(T') \left|\frac{dT}{dt}\right|^{-1} dT' = \frac{2}{\left|\frac{dT}{dt}\right|}\int_T^{T_N} U(T')\, dT'. \quad (3)$$

Eqs. 2 and 3 yield for $(T_N - T) \lesssim 5$(°C)

$$l(T_N, T) = \frac{2U(T)}{\left|\frac{dT}{dt}\right|}(T_N - T)\,[1 + C_1(T_N - T) + C_2(T_N - T)^2 \ldots.] \quad (4)$$

where

$$C_1 = (b_1 \ln 10)/2 \quad (5)$$

$$C_2 = (b_1 \ln 10)^2/6 - b_2(\ln 10)/3. \quad (6)$$

The solidified volume fraction, $\beta(T_S, T)$, at temperature T of a specimen which becomes fully solidified at temperature T_S is

$$\beta(T_S, T) = \int_T^{T_M} J(T_N)\cdot\alpha(T_S, T_N)\cdot\xi\cdot l(T_N, T)^3 \left|\frac{dT}{dt}\right|^{-1} dT_N \quad (7)$$

where

$$\alpha(T_S, T) = 1 - \beta(T_S, T) \quad (8)$$

and ξ is a parameter depending on the relationship between the ice crystal growth direction and the orientation of the ice crystal lattice axes. When the growth rate is independent of the growth direction $\xi = \pi/6$, whereas for ice crystal growth only along three axes perpendicular to one another and the same along all three axes $\xi = 1$.

At the solidification temperature, T_S, the specimen is fully solidified, i.e.,

$$\beta(T_S, T_S) = 1. \quad (9)$$

TABLE I
THE NUMERICAL VALUES OF PARAMETERS $a_1(T)$, $a_2(T)$, $b_1(T)$, AND $b_2(T)$

T/°C	−6	−10	−15	−20	−25	−30	−35	−40	−45
a_1/(°C)	~250	~50	~15	~5	2.0	1.6	1.2	0.8	0.6
$a_2 \cdot 10^2$/(°C^2)	~10^4	~10^3	~100	~10	4.1	4.1	4.1	2.2	2.2
$b_1 \cdot 10^2$/(°C)	0	0.43	2.8	4.0	5.1	5.6	6.4	7.1	7.4
$b_2 \cdot 10^3$/(°C^2)	6	2.4	1.2	1.2	0.5	0.8	0.7	0.3	~0.3

The numerical values of parameters $a_1(T)$, $a_2(T)$, $b_1(T)$ and $b_2(T)$ for pure water were obtained partly by using the analytical expressions for $J(T)$ and partly by reading off the ordinate, slope and curvature of the graphical presentations of $J(T)$ and $U(T)$ given by Riehle (1968).

Eqs. 8 and 9 yield

$$\alpha(T_S, T) = 1 - \frac{\beta(T_S, T)}{\beta(T_S, T_S)}. \quad (10)$$

Eqs. 1, 4, 7, and 10 yield

$$\alpha(T_S, T) = 1 - [10^{-(a_1 - 3b_1)(T - T_S) - (a_2 + 3b_2)(T - T_S)^2}] \cdot I_1(T)/I_1(T_S) \quad (11)$$

where

$$I_1(T) = \int_T^{T_M} \{10^{-a_1(T_N - T) - a_2(T_N - T)^2} \cdot \alpha(T_S, T_N) \cdot (T_N - T)^3 \cdot [1 + C_1(T_N - T) + C_2(T_N - T)^2]^3\} dT_N. \quad (12)$$

Change of integration variable to $\Delta T = T_N - T$ in Eq. 12 yields

$$I_1(T) = \int_0^{T_M - T} [10^{-a_1 \Delta T - a_2 \Delta T^2} \alpha(T_S, T + \Delta T) \cdot \Delta T^3 (1 + C_1 \Delta T + C_2 \Delta T^2)^3] d(\Delta T). \quad (13)$$

Because $a_1 \simeq 2$ (Table I) the integrand in $I_1(T)$ and $I_1(T_S)$ is negligible for $\Delta T \gtrsim 3$. For $T_M - T_S \geq 6$°C and $T_M - T \gtrsim 4$°C (Eq. 13) we therefore have

$$I_1(T) \simeq \int_0^{\infty} [10^{-a_1 \Delta T - a_2 \Delta T^2} \alpha(T_S, T + \Delta T) \cdot \Delta T^3 (1 + C_1 \Delta T + C_2 \Delta T^2)^3] d(\Delta T). \quad (14)$$

Parameter $\alpha(T_S, T)$ can be solved from Eqs. 11 and 14 using an iterative procedure where $\alpha_n(T_S, T)$ denotes the nth approximation of $\alpha(T_S, T)$

$$\alpha_0(T_S, T) = 1 \quad (15)$$

$$\alpha_n(T_S, T) = 1 - 10^{-(a_1 - 3b_1)(T - T_S) - (a_2 + 3b_2)(T - T_S)^2} \cdot I_2(T_S, T, n) \quad (16)$$

where

$$I_2(T_S, T, n) = \frac{\int_0^{\infty} [10^{-a_1 \Delta T - a_2 \Delta T^2} \cdot \alpha_{n-1}(T_S, T + \Delta T) \cdot \Delta T^3 \cdot (1 + C_1 \Delta T + C_2 \Delta T^2)^3] d(\Delta T)}{\int_0^{\infty} [10^{-a_1 \Delta T - a_2 \Delta T^2} \cdot \alpha_{n-1}(T_S, T_S + \Delta T) \cdot \Delta T^3 \cdot (1 + C_1 \Delta T + C_2 \Delta T^2)^3] d(\Delta T)}. \quad (17)$$

As a check of the validity of Eq. 16 $\alpha(T_S, T_S)$ may be calculated. Because the whole specimen is solidified for $T = T_S$, $\alpha(T_S, T_S)$ is expected to be equal to zero. For $n \geq 1$ Eq. 16 yields

$$\alpha_n(T_S, T_S) = 0 \quad (18)$$

as required.

The iterative procedure further yields

$$\alpha_1(T_S, T) = 1 - 10^{-(a_1 - 3b_1)(T - T_S) - (a_2 + 3b_2)(T - T_S)^2} \quad (19)$$

$$\alpha_2(T_S, T) = 1 - [1 - \alpha_1(T_S, T)] \cdot I_2(T_S, T, 2). \quad (20)$$

The numerical values given in Table I can be used to show that

$$1.00 \leq I_2(T_S, T, 2) \lesssim 1.06. \quad (21)$$

This means that the deviation between $\alpha_1(T_S, T)$ and $\alpha_2(T_S, T)$ is less than 2–3% for any T_S and T. Because it can be shown further that the iteration process converges rapidly, we will in the following use the approximation:

$$\alpha(T_S, T) \simeq \alpha_1(T_S, T). \quad (22)$$

$\alpha_1(T_S, T)$ calculated using the parameter values given in Table I is shown in Fig. 1.

For $T_S \lesssim -6$°C Eqs. 1, 2, 4, 7, 9, 19, and 22 yield

$$\frac{8 \cdot J(T_S) \cdot U^3(T_S)}{a_1^4 \cdot \left| \frac{dT}{dt} \right|^4} \cdot \xi \cdot I_3(T_S) = 1 \quad (23)$$

$$I_3(T_S) = \int_0^{(T_M - T_S)a_1} \{10^{-x - (a_2/a_1^2)x^2} - 10^{-[2 - 3(b_1/a_1)]x - [2(a_2/a_1^2) + (3b_2/a_1^2)]x^2}\} \cdot x^3 \cdot \left\{1 + \frac{C_1}{a_1} x + \frac{C_2}{a_1^2} x^2\right\}^3 dx. \quad (24)$$

Using the numerical values given in Table I it can be shown that

$$0.20 \lesssim I_3(T_S) \lesssim 0.25. \quad (25)$$

(See also Table II.)

Eq. 23 can be used to determine T_S for a given specimen cooling rate. Note that $J(T_S)$, $U(T_S)$ and a_1 generally are solute dependent.

Ice Crystal Size Distributions

The total number of ice crystals, $N(T_S)$, per unit volume in the solidified specimen

$$N(T_S) = \int_{T_S}^{T_M} P_N(T_S, T) dT \quad (26)$$

where $P_N(T_S, T)$ is the number of ice crystals formed per unit volume in

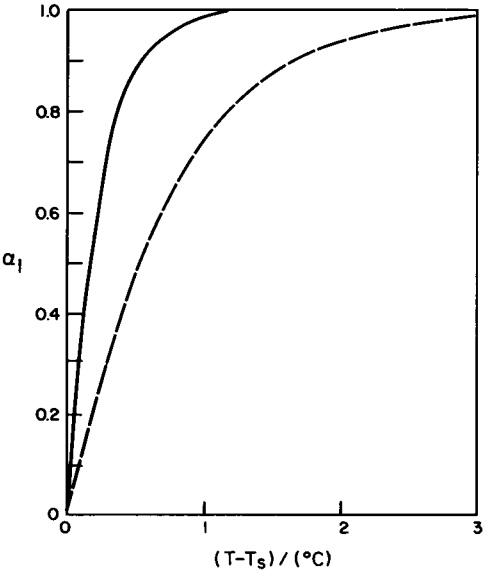

FIGURE 1 The unsolidified volume-fraction, α_1, of the specimen vs. T-T_S for solidification temperature $T_S = -25$(°C) (—), and $T_S = -40$(°C) (-----).

TABLE II
THE NUMERICAL VALUES OF INTEGRALS $I_3(T_S)$, $I_4(T_S)$, AND $I_5(T_S)$*

T_S(°C)	−6	−10	−15	−20	−25	−30	−35	−40	−45
$I_3(T_S)$	0.20	0.20	0.20	0.20	0.21	0.21	0.21	0.25	0.23
$I_4(T_S)$	0.22	0.22	0.22	0.21	0.21	0.20	0.19	0.18	0.15
$I_5(T_S)$	1.8	1.8	1.8	1.8	1.9	1.9	2.0	2.1	2.1

*Obtained using the numerical values of a_1, a_2, b_1, and b_2 given in Table I.

the temperature interval T, $T + dT$

$$P_N(T_S, T) = J(T) \cdot \alpha(T_S, T) \cdot \left|\frac{dT}{dt}\right|^{-1}. \quad (27)$$

Eqs. 1, 22, 26, and 27 yield

$$N(T_S) \simeq \frac{J(T_S)}{a_1 \cdot \left|\frac{dT}{dt}\right|} \cdot I_4(T_S) \quad (28)$$

$$I_4(T_S) = \int_0^{(T_M - T_S)a_1} \{10^{-x-(a_2/a_1^2)x^2} - 10^{-[2-3(b_1/a_1)]x-[2(a_2/a_1^2)+(3b_2/a_1^2)]x^2}\}\, dx. \quad (29)$$

For the numerical values given in Table I

$$0.15 \lesssim I_4(T_S) \lesssim 0.22. \quad (30)$$

(See also Table II.)

The relative number of ice crystals, $P_N(l)$, with diameter in the interval l, $l + dl$

$$P_N(l) = \frac{P_N[T_S, T(l)] \cdot \left|\frac{dT}{dl}\right|}{N(T_S)}. \quad (31)$$

Ignoring terms of order $(T_N - T)^3$ and higher, and introducing

$$\lambda \equiv \frac{2U(T)}{a_1 \cdot \left|\frac{dT}{dt}\right|} \quad (32)$$

Eq. 4 yields

$$T_N - T = \frac{1}{2C_1}\left[\sqrt{1 + 4\frac{C_1}{a_1}\left(\frac{1}{\lambda}\right)} - 1\right] \quad (33)$$

$$\left|\frac{dT}{dl}\right| = \frac{1}{\lambda a_1}\left[1 + 4\frac{C_1}{a_1}\left(\frac{l}{\lambda}\right)\right]^{-1/2}. \quad (34)$$

Parameter λ is a characteristic length of the physical problem being analyzed. It is convenient to express other lengths, such as ice crystal size, relative to this characteristic length. Fig. 2 shows the numerical value of λ vs. T for pure water using the parameter values given in Table I. Note that $U(T)$ and a_1 are generally solute dependent.

Eqs. 1, 18, 27, 28, 31, and 34 yield

$$P_N\left(\frac{l}{\lambda}\right) = \frac{10^{-a_1x-a_2x^2} - 10^{-(2a_1-3b_1)x-(2a_2+3b_2)x^2}}{I_4(T_S) \cdot \sqrt{1 + 4\frac{C_1}{a_1}\left(\frac{l}{\lambda}\right)}} \quad (35)$$

where

$$x = \frac{1}{2C_1}\left[\sqrt{1 + 4\frac{C_1}{a_1}\left(\frac{l}{\lambda}\right)} - 1\right] \quad C_1 \neq 0$$

$$x = \frac{1}{a_1}\left(\frac{l}{\lambda}\right) \quad C_1 = 0. \quad (36)$$

Number average ice crystal diameter using the numerical values given in Table I for $T_S = -25$°C.

$$\left(\frac{\bar{l}}{\lambda}\right)_N = \int_0^\infty \left(\frac{l}{\lambda}\right) \cdot P_N\left(\frac{l}{\lambda}\right) d\left(\frac{l}{\lambda}\right) \simeq 0.67. \quad (37)$$

The solidified specimen volume fraction, $P_V(l/\lambda)$, made up of ice crystals with diameter in the interval (l/λ), $(l/\lambda) + d(l/\lambda)$ is given by

$$P_V\left(\frac{l}{\lambda}\right) = \frac{\left(\frac{l}{\lambda}\right)^3 \cdot P_N\left(\frac{l}{\lambda}\right)}{\int_0^\infty \left(\frac{l}{\lambda}\right)^3 \cdot P_N\left(\frac{l}{\lambda}\right) d\left(\frac{l}{\lambda}\right)}. \quad (38)$$

Using the numerical values given in Table I the size distributions $P_N(l/\lambda)$ and $P_V(l/\lambda)$ are shown for $T_S = -25$°C in Fig. 3. The volume average ice crystal diameter is given by

$$\left(\frac{\bar{l}}{\lambda}\right)_V = I_5(T_S) = \int_0^\infty \left(\frac{l}{\lambda}\right) \cdot P_V\left(\frac{l}{\lambda}\right) \cdot d\left(\frac{l}{\lambda}\right). \quad (39)$$

Numerical values of $I_5(T_S)$ obtained using the parameter values given in Table I are shown in Table II.

For $l/\lambda \approx 1$ Eq. 33 becomes

$$T_N - T_S \simeq \frac{1}{a_1} \cdot \frac{l}{\lambda}. \quad (40)$$

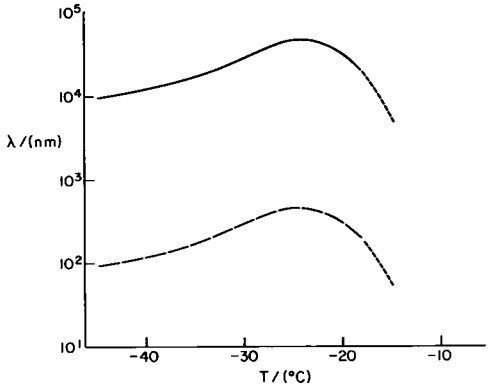

FIGURE 2 Parameter λ for pure water vs. temperature T for specimen cooling rate, $|dT/dt|$, equal 10^3 (°C/s) (—), and 10^5 (°C/s) (-----).

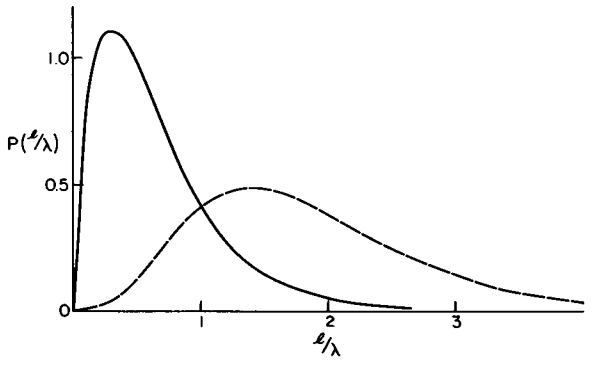

FIGURE 3 The ice crystal size distributions $P_N(l/\lambda)$ (—), and $P_V(l/\lambda)$ (-----) vs. l/λ for $T_S = -25(°C)$.

The volume average of $T_N - T_S$

$$\overline{(T_N - T_S)_V} \simeq \frac{1}{a_1} \cdot \left(\frac{\bar{l}}{\lambda}\right)_V. \tag{41}$$

Table II and Eqs. 40 and 41 yield for $T_S = -25°C$

$$\overline{(T_N - T_S)_V} \simeq 0.9 \quad (°C) \tag{42}$$

which means that the nucleation of the average solidified specimen ice crystal took place only ~0.9°C above the solidification temperature T_S.

During freeze fracture of a specimen, the average numbers, $P_N^A(1)$, of ice crystals with diameter in the interval 1, 1 + d1 fractured per unit fracture plane area are

$$P_N^A(l) = P_N(l) \cdot l. \tag{43}$$

The relative number, $P_N^A(r)$, of ice crystal fracture planes with radius r in the interval r, $r + dr$ is given by

$$P_N^A(r) = \frac{\int_{2r}^{\infty} P_N(l) \cdot l \cdot P(l; r)dl}{\int_0^{\infty} dr \int_{2r}^{\infty} P_N(l) \cdot l \cdot P(l; r)\, dr} \tag{44}$$

where $P(l; r)$ is the probability of getting an ice-crystal fracture plane with radius r provided that the fracture goes through an ice-crystal with diameter l. When the ice crystal growth rate is the same in all directions relative to the ice crystal axes (spherical ice crystals)

$$P(l; r)_I = \frac{2r}{l\sqrt{(l/2)^2 - r^2}}. \tag{45}$$

For cylindrical ice crystals with diameter and length being equal and with the cylinder symmetry axis perpendicular to the fracture plane

$$P(l; r)_{II} = \delta(l - 2r) \tag{46}$$

where $\delta(x)$ is Dirac's delta function.

The area fraction of the specimen freeze-fracture plane made up of ice crystals with fracture plane radius in the interval r, $r + dr$

$$P_A^A(r) = \frac{r^2 \cdot P_N^A(r)}{\int_0^{\infty} r^2 \cdot P_N^A(r)\, dr}. \tag{47}$$

Eqs. 44 and 47 yield

$$P_A^A\left(\frac{r}{\lambda}\right) = \frac{\left(\frac{r}{\lambda}\right)^2 \int_{2r/\lambda}^{\infty} P_N\left(\frac{l}{\lambda}\right) \cdot \left(\frac{l}{\lambda}\right) \cdot P\left(\frac{l}{\lambda}; \frac{r}{\lambda}\right) d\left(\frac{l}{\lambda}\right)}{\int_0^{\infty} \left(\frac{r}{\lambda}\right)^2 \left[\int_{2r/\lambda}^{\infty} P_N\left(\frac{l}{\lambda}\right) \cdot \left(\frac{l}{\lambda}\right) \cdot P\left(\frac{l}{\lambda}; \frac{r}{\lambda}\right) d\left(\frac{l}{\lambda}\right)\right] d\left(\frac{r}{\lambda}\right)}. \tag{48}$$

Eqs. 35, 45, and 48 yield

$$P_A^A\left(\frac{r}{\lambda}\right)_I \propto \left(\frac{r}{\lambda}\right)^3 \int_{2r/\lambda}^{\infty} [10^{-a_1 x - a_2 x^2} - 10^{-(2a_1 - 3b_1)x - (2a_2 + 3b_2)x^2}] \cdot \left(1 + 4\frac{C_1}{a_1}\frac{l}{\lambda}\right)^{-1/2} \cdot \left[\left(\frac{l}{2\lambda}\right)^2 - \left(\frac{r}{\lambda}\right)^2\right]^{-1/2} \cdot d\left(\frac{l}{\lambda}\right) \tag{49}$$

where x is given by Eq. 36.

Eqs. 35, 46, and 48 yield

$$P_A^A\left(\frac{r}{\lambda}\right)_{II} \propto \left(\frac{r}{\lambda}\right)^3 \cdot [10^{-a_1 x - a_2 x^2} - 10^{-(2a_1 - 3b_1)x - (2a_2 + 3b_2)x^2}] \cdot \left(1 + 8\frac{C_1}{a_1}\frac{r}{\lambda}\right)^{-1/2} \tag{50}$$

where

$$x = \frac{1}{2C_1}\left[\sqrt{1 + 8\frac{C_1}{a_1}\left(\frac{r}{\lambda}\right)} - 1\right]. \tag{51}$$

The distributions $P_A^A(r/\lambda)_I$ and $P_A^A(r/\lambda)_{II}$ for $T_s \simeq -25°C$ are shown in Fig. 4. In Fig. 5 is depicted $P_A^A(r/\lambda)_I$ and the experimentally determined $P_A^A(r/\eta)_{exp}$ from the freeze-fracture electron micrograph presented in Fig. 6. The radius r for the fracture plane of an ice crystal in Fig. 6 is defined as

$$r = \sqrt{A_{exp}/\pi} \tag{52}$$

where A_{exp} is the experimentally determined fracture area of the ice crystal using a planiometer. Parameter η has been chosen so that

$$\int_0^{\infty} \left(\frac{r}{\lambda}\right) P_A^A\left(\frac{r}{\lambda}\right)_I d\left(\frac{r}{\lambda}\right) \simeq \int_0^{\infty} \left(\frac{r}{\eta}\right) P_A^A\left(\frac{r}{\eta}\right)_{exp} d\left(\frac{r}{\eta}\right). \tag{53}$$

This corresponds to $\lambda = 1200$ nm for the specimen shown in Fig. 6.

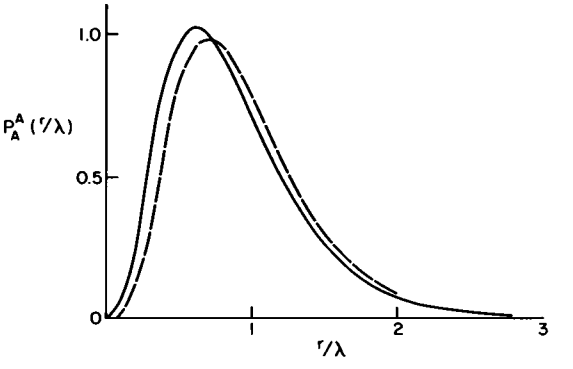

FIGURE 4 The ice crystal size distribution in the specimen fracture plane $P_A^A(r/\lambda)_I$(—), and $P_A^A(r/\lambda)_{II}$(-----).

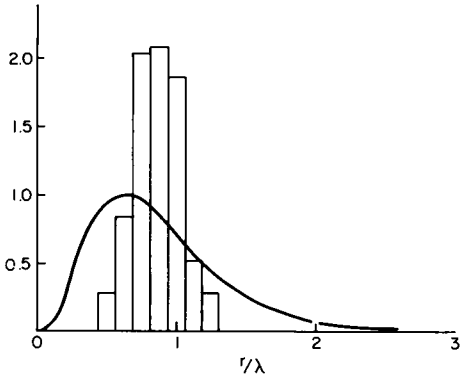

FIGURE 5 The size distribution of the ice crystal fracture areas $P_A^A(r/\lambda)_I$(——) at $T_S = -25°C$. The fracture area size distribution of the freeze-etch electron micrograph shown in Fig. 6 is presented as columns.

Average Ice Crystal Size Cooling Rate Dependence

The coefficient $k(T_S)$ of the expression

$$\overline{\left(\frac{\overline{\Delta l}}{l}\right)}_V = -k(T_S)\frac{\Delta\left|\frac{dT}{dt}\right|}{\left|\frac{dT}{dt}\right|} \tag{54}$$

has been derived in the Appendix. The numerical values of $k(T_S)$ vs. T_S using the numerical values of a_1, b_1, I_3 and I_5 given in Tables I and II are shown in Fig. 7.

DISCUSSION

The approximate expression for $J(T)$ and $U(T)$ (Eqs. 1 and 2) are reasonably accurate for $T_N - T \lesssim 5°C$. Fig. 1 and Eq. 42 show that the major part of the specimen solidification takes place within a temperature interval of <2–3°C. The use of Eqs. 1 and 2 is therefore well justified for the temperature interval where most of the ice crystal nucleation and growth take place.

The experimental size distribution $P_A^A(r)$ shown in Fig. 5 has approximately the same form as the distribution calculated theoretically. A characteristic of the theoretical and experimental size distribution is that they are both rather narrow. A large majority of the individual ice crystals in the fracture plane are larger than half the mean size and smaller than twice the mean size. The theoretical and experimental size-distributions shown in Fig. 5 have maxima for somewhat different values of r/λ. The reason for this is that the theoretical distribution does not fall off as fast with increasing r/λ for $r/\lambda > 1$ as the experimental distribution does. To get adequate sampling statistics for large ice crystals much larger fracture areas than shown in Fig. 6 must be analyzed. Experimentally obtained size distributions using a small fracture plane sampling area will on average show relatively fewer large ice crystals than a distribution obtained using a larger fracture plane sampling area. This sampling error increases with increasing

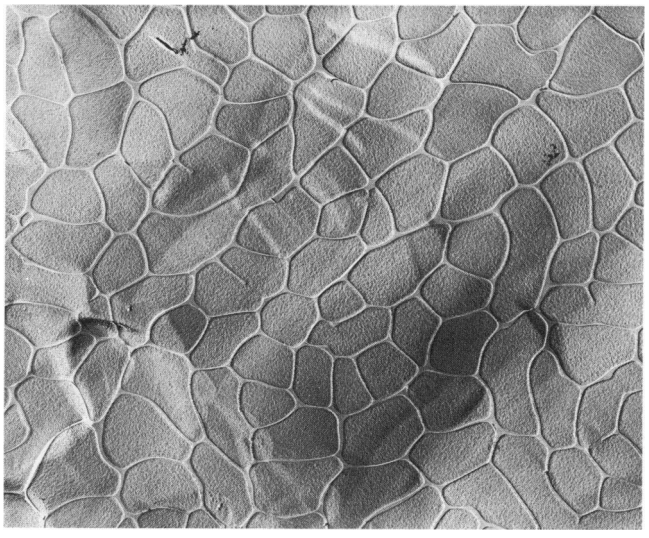

FIGURE 6 Freeze-etch electron micrograph of a 5% glycerol solution frozen by conventional manual dipping of the specimen into partly solidified Freon 22 (Norgas AS, Oslo). The ~1-μl drop-shaped specimen was mounted on a hat-shaped copper specimen holder. Specimen fracturing and etching was carried out at −100°C. The etch time was 1 min, 6,000×.

r/λ and probably is the main reason for the apparent discrepancy between the theoretical and the experimental ice crystal size distribution for large r/λ found in Fig. 5. When $\alpha(T_S, T) \lesssim 0.3$, the specimen ice crystals on average, begin to touch one another. This phenomenon has not been taken into account in our theoretical analysis, and may be expected to result in a slightly broader size distribution than predicted. Another effect for low α is increased solute concentration in the unsolidified parts of the specimen, which will tend to speed up the last part of the solidification process since increased solute concentration generally increases the nucleation rate. This will tend to make the experimentally determined size distribution somewhat narrower than predicted by our analysis. At what α this effect becomes dominant depends upon the initial solute concentration. This phenomenon is closely

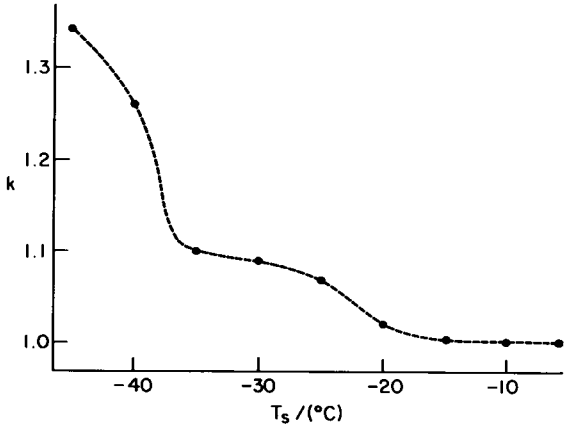

FIGURE 7 Coefficient $k(T_S)$ vs. T_S for pure water.

related to the formation of the so-called eutectic lines shown in Fig. 6. The presented theoretical analysis does not include this mechanism. However, for 5% glycerol solutions (Fig. 6), for example, the eutectic lines account for <15% of the specimen volume and thus only to a minor extent affect the total ice crystal size distribution. The experimentally determined ice crystal size distribution shown in Fig. 5 is thus reasonably well accounted for by our theoretical analysis, which indicates that the average ice crystal size for pure water will be reduced by ~10% at moderate cooling rates and ~15% at high cooling rates, when the cooling rate is increased by 10%. Using freeze-etch electron microscopy for estimating the average ice crystal size, Riehle (1968) obtained data for 5% glycerol solution indicating a 5–10% reduction in average ice crystal size at moderate ($\sim 10^3$ °C s^{-1}) and a 10–20% reduction at high ($\sim 10^6$ °C s^{-1}), rates of cooling as a result of a 10% increase in cooling rate. Considering the uncertainties of the numerical values of parameters $a_1(T)$, $a_2(T)$, $b_1(T)$ and $b_2(T)$ and of the experimental data the agreement between the theoretical and experimental results is reasonable.

APPENDIX

Average Ice Crystal Size Cooling Rate Dependence

Eqs. 32 and 39 yield

$$\overline{l_v} = \frac{2U(T_S)}{a_1(T_S) \cdot \left|\frac{dT}{dt}\right|} \cdot I_5(T_S) \tag{A1}$$

$$\left(\frac{\overline{\Delta l}}{l}\right)_v = \frac{\Delta U(T_S)}{U(T_S)} + \frac{\Delta I_5(T_S)}{I_5(T_S)} - \frac{\Delta a(T_S)}{a(T_S)} - \frac{\Delta\left|\frac{dT}{dt}\right|}{\left|\frac{dT}{dt}\right|} \tag{A2}$$

$$\left(\frac{\overline{\Delta l}}{l}\right)_v = -\left\{1 - \left[\frac{1}{U(T_S)}\frac{dU(T_S)}{dT_S} + \frac{1}{I_5(T_S)}\frac{dI_5(T_S)}{dT_S} - \frac{1}{a_1(T_S)}\frac{da_1(T_S)}{dT_S}\right] \cdot \frac{dT_S}{d\left|\frac{dT}{dt}\right|} \cdot \left|\frac{dT}{dt}\right|\right\} \cdot \frac{\Delta\left|\frac{dT}{dt}\right|}{\left|\frac{dT}{dt}\right|} \tag{A3}$$

From Eq. 23

$$\left|\frac{dT}{dt}\right| \frac{dTs}{d\left|\frac{dT}{dt}\right|} = 4\Big/\left[\frac{1}{J(T_S)}\frac{dJ(T_S)}{dT_S} + \frac{3}{U(T_S)}\frac{dU(T_S)}{dT_S} + \frac{1}{I_3(T_S)}\frac{dI_3(T_S)}{dT_S} - \frac{4}{a_1(T_S)}\frac{da_1(T_S)}{dT_S}\right]. \tag{A4}$$

From Eqs. A3 and A4

$$\left(\frac{\Delta l}{l}\right)_v = -k(T_S)\frac{\Delta\left|\frac{dT}{dt}\right|}{\left|\frac{dT}{dt}\right|} \tag{A5}$$

$$k(T_s) = 1 - 4\left[\frac{1}{U(T_S)}\frac{dU(T_S)}{dT_S} + \frac{1}{I_5(T_S)}\frac{dI_5(T_S)}{dT_S} - \frac{1}{a_1(T_S)}\frac{da_1(T_S)}{dT_S}\right]\Big/\left[\frac{1}{J(T_S)}\frac{dJ(T_S)}{dT_S} + \frac{3}{U(T_S)}\frac{dU(T_S)}{dT_S} + \frac{1}{I_3(T_S)}\frac{dI_3(T_S)}{dT_S} - \frac{4}{a_1(T_S)}\frac{da_1(T_S)}{dT_S}\right]. \tag{A6}$$

From Eq. 1

$$\frac{1}{J(T_S)}\frac{dJ(T_S)}{dT_S} = -(\ln 10) \cdot a_1(T_2). \tag{A7}$$

From Eq. 2

$$\frac{1}{U(T_S)}\frac{dU(T_S)}{dT_S} = +(\ln 10) \cdot b_1(T_S). \tag{A8}$$

REFERENCES

Brügeller, P., and E. Mayer. 1980. Complete vitrification in pure liquid water and dilute aqueous solutions. *Nature (Lond.).* 288:569–571.

Gibbs, W. 1928. Collected Works. Vol. I. Longman, Inc., New York. 314–331.

Mazur, P. 1966. Basis of freezing injury. *In* Cryobiology. H. T. Merymann, editor. Academic Press, Inc., New York. 214–315.

Moor, H. 1964. Die Gefrierätzung lebender Zellen und ihre Anwendung in der Elektronen Mikroskopie. *Z. Zellforsch. Mikrosk. Anat.* 62:546–580.

Riehle, U. 1968. Ueber die Vitrifizierung verdünnter wässriger Lösungen. Diss. n° 4271. Eidgenössiche Technische Hochschule Zürich, Juris Druck & Verlag, Zürich. 1–133.

Venkatesh, C. G., S. A. Rice and A. H. Narten. 1974. Amorphous solid water: an x-ray diffraction study. *Science (Wash. D.C.).* 186:927–928.